ACS APPLIED MATERIALS & INTERFACES

Research Article

Cite This: ACS Appl. Mater. Interfaces 2018, 10, 37679−37684

www.acsami.org

Reduction and Increase in Thermal Conductivity of Si Irradiated with Ga^+ via Focused Ion Beam

S. Alaie,[†] M. G. Baboly,[‡] Y.-B. Jiang,[§] S. Rempe,[#] D. H. Anjum,[▽] S. Chaieb,[○,◆,¶] B. F. Donovan,[⋈] A. Giri,[⋈] C. J. Szwejkowski,[⋈] J. T. Gaskins,[⋈] M. M. M. Elahi,[∥] D. F. Goettler,[⊥] J. Braun,[⋈] P. E. Hopkins,[⋈,⧖,●] and Z. C. Leseman*[,¤]

[†]Department of Radiology, Weill Cornell Medicine, Cornell University, New York, New York 10065, United States

[‡]Department of Engineering, University of Jamestown, Jamestown, North Dakota 58405, United States

[§]Department of Chemical and Biological Engineering, [∥]Department of Electrical and Computer Engineering, and [⊥]Department of Mechanical Engineering, University of New Mexico, Albuquerque, New Mexico 87131, United States

[#]Sandia National Laboratories, Albuquerque, New Mexico 87123, United States

[▽]Advanced Nanofabrication, Imaging, and Characterization Lab and [○]Division of Biological and Environmental Sciences and Engineering, King Abdullah University of Science and Technology, Thuwal 23955-6900, Kingdom of Saudi Arabia

[◆]Lawrence Berkeley National Laboratory, Berkeley, California 94720, United States

[¶]Materials and Structures Laboratory, Tokyo Institute of Technology, Yokohama 226-8503, Japan

[⋈]Department of Physics, United States Naval Academy, Annapolis, Maryland 21402, United States

[⋈]Department of Mechanical and Aerospace Engineering, [⧖]Department of Materials Science and Engineering, and [●]Department of Physics, University of Virginia, Charlottesville, Virginia 22904, United States

[¤]Department of Mechanical and Nuclear Engineering, Kansas State University, Manhattan, Kansas 66506, United States

ABSTRACT: Focused ion beam (FIB) technology has become a valuable tool for the microelectronics industry and for the fabrication and preparation of samples at the micro/nanoscale. Its effects on the thermal transport properties of Si, however, are not well understood nor do experimental data exist. This paper presents a carefully designed set of experiments for the determination of the thermal conductivity of Si samples irradiated by Ga^+ FIB. Generally, the thermal conductivity decreases with increasing ion dose. For doses of $>10^{16}$ (Ga^+/cm^2), a reversal of the trend was observed due to recrystallization of Si. This report provides insight on the thermal transport considerations relevant to engineering of Si nanostructures and interfaces fabricated or prepared by FIB.

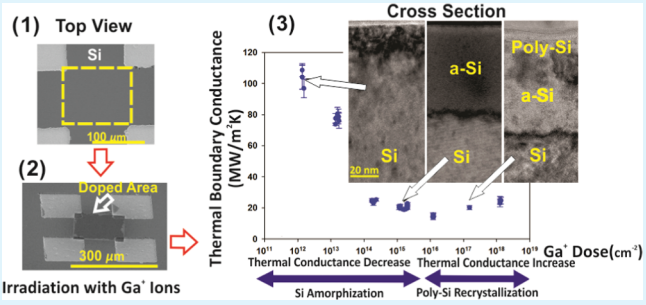

KEYWORDS: *focused ion beam (FIB), thermal conductivity, gallium, irradiated, nanostructures, time-domain thermoreflectance (TDTR)*

INTRODUCTION

Over the last two decades, the thermal conductivity of different nano/micro structured silicon samples has been extensively investigated for a range of purposes. For example, to understand the physics of phonon thermal transport at the nanoscale, silicon films with different thicknesses have been experimentally and theoretically investigated.[1−3] Additionally, the possibility of using silicon as a thermoelectric material has been confirmed.[4−6] Accordingly, manipulation of the thermal conductivity of silicon, with minimal alteration of the electrical properties, has become an active area of research.[7−9] To fabricate different Si structures, photolithography[7,10] and e-beam lithography[4,5] techniques have been employed. Recently, gallium-focused ion beam (FIB)[8,10] has been used as a promising alternative. However, it is known that FIB can potentially damage, dope, or roughen silicon surfaces.[11−13] Therefore, in this work, a carefully designed set of experiments to determine the effects of FIB, and resulting Ga ion (Ga^+) implantation, on the thermal conductivity of Si is undertaken.

Though the thermal conductivity of silicon with various (small) dimensions and doping has been previously investigated, the effect of gallium impurities on silicon's thermal conductivity has not been previously studied. More specifically, the thermal conductivities of thin Si films,[1−3] Si nanowires,[6,14]

Received: July 27, 2018
Accepted: October 3, 2018
Published: October 3, 2018

DOI: 10.1021/acsami.8b11949
ACS Appl. Mater. Interfaces 2018, 10, 37679−37684

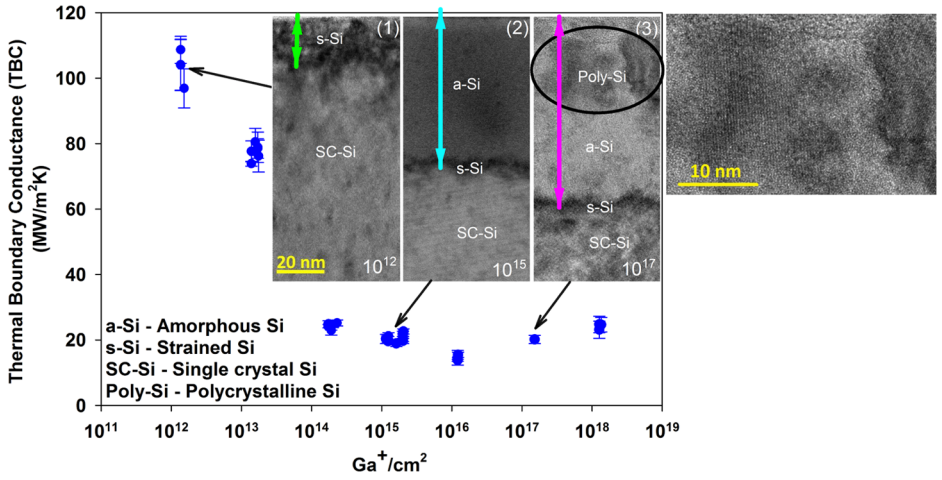

Figure 1. Thermal conductance of Ga^+-irradiated region versus the dose of gallium induced by FIB. Due to the small thickness of the Ga^+-irradiated region (<70 nm thick), the conductance is reported as an effective thermal boundary conductance across the Al/Ga^+-irradiated volume/Si interfacial region[27] and by definition also includes the thermal boundary conductances across the Al/Ga^+-irradiated region and Ga^+-irradiated region/Si interfaces. Insets (1)−(3) are transmission electron microscope (TEM) images demonstrating the morphological evolution of the irradiated Si for increasing dose. The tops of the insets are the surface of the Si that were irradiated with Ga^+; irradiation was perpendicular to this surface. The circled portion of inset (3) is further magnified to more clearly show the existence of polycrystals of Si for higher doses. For the insets, arrows have been drawn to show the different morphological regions of the Si. For the 10^{12} Ga^+/cm^2, the green arrow indicates the strained Si (s-Si). For the 10^{15} Ga^+/cm^2, the cyan arrow shows the a-Si. And for the 10^{17} Ga^+/cm^2, the magenta arrows show the depth of the a-Si.

patterned Si films,[4,10] and other Si structures[15] have been the subject of prior work. The literature established that at smaller dimensions the boundary scattering of phonons dominates, which results in a considerable reduction of thermal conductivity (~2 W/(m K)).[4] In addition to the size effect, effects of different dopants and mass impurities, such as phosphorous[16,17] and germanium,[18−21] on the thermal conductivity of silicon have been studied. Most remarkably, it is shown that $Si_xGe_{(1-x)}$ can feature a thermal conductivity as low as ~9 W/(m K) in bulk and when combined with the size effect it can reduce to ~2 W/(m K).[18] However, the effects of gallium as a dopant or mass impurity on the thermal conductivity of silicon are yet unknown, regardless of its common occurrence in FIB-processed silicon.

Ga^+ FIB has been widely employed in milling,[13,22,23] imaging,[9,24] and affixing nanosamples.[9,25] FIB is a versatile tool for milling thin films with submicron resolution. The FIB's spot size can be as small as 5−7 nm[26] for milling materials and it can also be used to deposit a variety of materials to fabricate sophisticated nanostructures.[26] For thermal applications, it has been employed to fabricate phononic crystals in silicon thin films.[13] Additionally, FIB is used for imaging nano/micro samples while they are handled for thermal characterization[24,25] and is employed for the deposition of materials for affixing nano/micro samples to microelectromechanical structures for thermal characterization.[9,23] However, despite its widespread use as a nanoscience tool, the FIB can potentially have a negative impact due to implantation of Ga^+ into samples that introduce defects and impurities into the sample.

In this work, the thermal conductance and the equivalent thermal conductivity of regions of single-crystal Si wafers irradiated by Ga^+ FIB are studied. To fully understand the effects of the implanted Ga^+, samples with different doses ranging from 10^{12} to 10^{18} Ga^+/cm^2 are studied. After irradiation, samples are coated with a thin layer of aluminum for characterization by time-domain thermoreflectance (TDTR). The thermal properties gathered by this technique are crucial in understanding the thermal effects of FIB-induced Ga dopants on micro/nanosamples of Si. Results may be extrapolated to other material systems.

RESULTS AND DISCUSSION

The thermal conductance across the Ga^+-irradiated silicon region is reported in Figure 1 for different doses. In practice, due to the small thickness of the Ga^+-irradiated region (<70 nm thick), the conductance is reported as an effective thermal boundary conductance (TBC) across the Al/Ga^+-irradiated volume/Si interfacial region,[27] and by definition also includes the thermal boundary conductances across the Al/Ga^+-irradiated region and Ga^+-irradiated region/Si interfaces. However, the variation in the measured conductance clearly demonstrates the role of the Ga^+ irradiation process on the decrease in thermal conductivity of the near-surface irradiated region. The measured TBC drops for doses from 10^{12} to 10^{14} Ga^+/cm^2, whereas a trend of saturation occurs for the doses ranging from 10^{14} to 10^{16} Ga^+/cm^2. For higher doses, >10^{16}/cm^2, an increase is observed in the TBC.

The trend of decreasing followed by increasing TBC is explained by the morphological evolution of the sample shown in the insets of Figure 1. For low doses of Ga^+, the single-crystal Si (SC-Si) lattice becomes strained as indicated by the darker (black) region of the 10^{12} Ga^+/cm^2 dose inset, inset (1). Lattice distortion is known to modify the phonon dispersion and phonon scattering rates and thus the thermal conductivity of Si and other semiconductors and dielectrics.[28−30] Upon further irradiation, the Si becomes amorphous as seen in the inset corresponding to a dose of 10^{15} Ga^+/cm^2, inset (2). Amorphous materials have lower thermal conductivities than their crystalline counterparts in semiconducting materials, such as Si, because these rely on the exchange of vibrational energy carried through the crystalline lattice. For increased doses, the Si changes into polycrystalline Si, as seen in the TEM inset for a dose of 10^{17} Ga^+/cm^2, inset (3). As the sample returns from amorphous to crystalline (polycrystalline), an increase in the effective TBC is measured due to the Si regaining some levels of crystallinity, the circled region of inset (3).

DOI: 10.1021/acsami.8b11949
ACS Appl. Mater. Interfaces 2018, 10, 37679−37684

Figure 2 shows the normalized effective thermal conductivity of the implanted region versus the dose of gallium. The

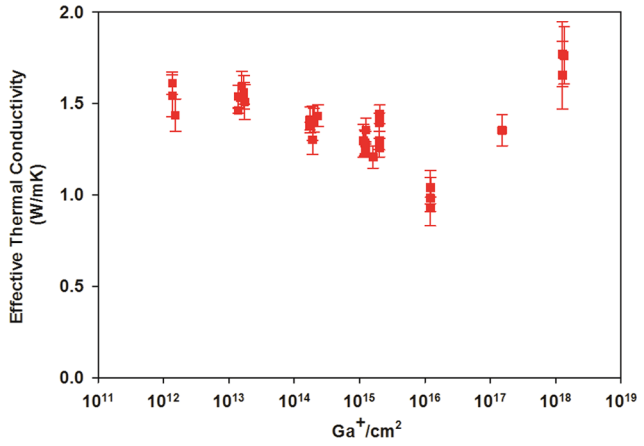

Figure 2. Effective out-of-plane thermal conductivity of irradiated volume of Si versus the dose of Si dopant.

thermal conductivity here is the effective thermal conductivity of the irradiated Si, which is the product of the measured TBC and the thickness of the irradiated regions, as determined by TEM cross-sections similar to those seen in the insets of Figure 1. The thermal conductivity follows a power trend (linear on a linear log scale) for a regime between the doses of 10^{13} and 10^{17} Ga^+/cm^2. The thermal conductivity again increases for a dose beyond 10^{17} Ga^+/cm^2, which is near the dose required for milling[31] (removing of material). It is notable that the effective thermal conductivity of the implanted region is approximately 2 orders of magnitude lower than the thermal conductivity of Si and consistent to what has been reported for thin (<100 nm thick) films of pure a-Si, which have been measured to be between 1 and 2 W/(m K).[32,33]

The most interesting observation found in this work is that polycrystalline Si recrystallizes for doses greater than 10^{16} Ga^+/cm^2. Recrystallization occurs for higher doses due to the thermal history of the sample. Temperatures of the interaction volume of the Ga^+ beam are in excess of 1000 K, as determined using an energy balance approach and the heat equation.[34] FIB interacts with a sample as a beam that rasters an area points by point. Therefore, irradiation of adjacent points may induce a time at elevated temperatures in addition to that of the direct beam exposure. The intrinsic crystallization temperature for a-Si is ~900 K,[35] as determined in parallel work that uses short pulse lasers to crystallize a-Si.[36] Note that the absorbed laser energy during TDTR measurements of the samples in this study raises their temperature by <1 K[37] and is not responsible for the recrystallization.

Previously, it was believed that the maximum temperature experienced by Si samples when milled by Ga^+ FIB was only a few degrees[38] over ambient and that once the semiconducting material becomes amorphous it remains amorphous. This is due to the common assumption that the thermal conductivity of the Si under the FIB is that of the bulk material.[38] Inset (2) of Figure 1 clearly shows that the material under the FIB is amorphous in nature. For thin films of a-Si of the thickness in the insets of Figure 1, reported values are more than 100 times less than that of their bulk counterparts,[32,39] which is what leads to the greater than 1000 K temperature excursions. Note that other researchers have experienced "extreme micro-structural modifications" in fine grained metals[40] when using Ga^+ FIBs. The TEM, scanning transmission electron microscopy, and Electron backscatter diffraction methods have been used to show that polycrystalline Cu (face-centered cubic) when exposed to Ga^+ FIB experiences changes in crystal orientation, grain size, and the formation of intermetallic compounds.[41,42] Similar results were noticed in Au and Ni (body-centered cubic) metals as well[40,43] due to thermal spikes.[42] Note that Cu, Au, and Ni all have lower recrystallization temperatures than Si.[35,44] It has also been shown that grain growth in the metallic samples has preferential growth directions that are dictated by the channeling of ions through their crystalline structures. The zoomed in view of Figure 3 shows some evidences of orientation-directed growth of the Si polycrystals along the direction of Ga^+ irradiation.[42]

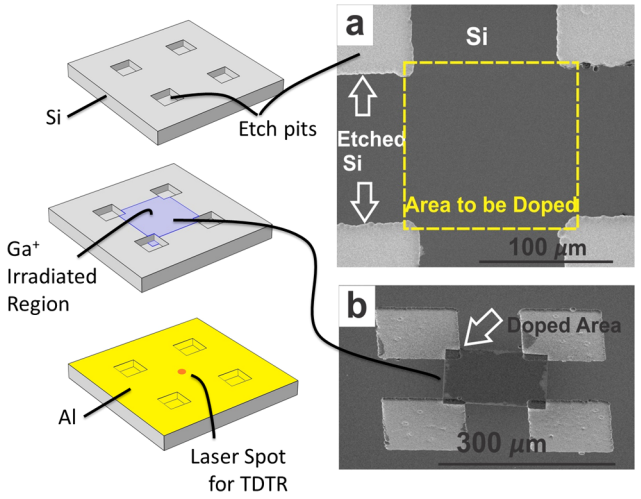

Figure 3. From top to bottom in left column: (a) bare Si with fabricated alignment marks, (b) exposure to Ga^+ FIB, deposition of Al and characterization using TDTR.

CONCLUSIONS

In this report, the thermal conductance of Si regions irradiated with Ga^+ FIB has been measured using TDTR and their morphology characterized using cross-sectional TEM. It was found that irradiation of Si with Ga^+ lowers the thermal conductivity of Si up to a dose of ~10^{16} Ga^+/cm^2. Over this range of doses, TEM cross-sections reveal the evolution of the morphology from crystalline to amorphous. For doses >10^{16} Ga^+/cm^2, the thermal conductivity increases due to the recrystallization of Si. This is due to the temperature of Si reaching an excess of 1000 K, well above the intrinsic crystallization temperature of amorphous Si. This work provides crucial information for engineering of thermal samples at the nano/microscale in applications where gallium FIB is involved.

METHODS

Sample Preparation. Single crystalline Si, 525 μm total thickness, was exposed to Ga^+ FIB with different currents in the manner depicted in Figure 3. An FEI, Quanta 3D dual beam FIB/scanning electron microscopy (SEM) was used to expose the samples with an accelerating voltage of 30 kV. The insets of Figure 3a,b show the SEM images before and after the irradiation with Ga^+. Different nominal currents were chosen (1.5 pA, 20 pA, 1 nA, and 5 nA) to cover the

DOI: 10.1021/acsami.8b11949
ACS Appl. Mater. Interfaces 2018, 10, 37679−37684

entire range of doses studied. However, the actual current received by the sample was calibrated with a Faraday cup for each current and used in the calculation of dosage. For each current, several different exposure times are used to attain different dosages. Knowing the time span of the exposure, current received by the sample, and the area for the exposure, the dose of Ga ions for each sample was calculated.

Thermal Characterization. Time-domain thermoreflectance (TDTR) was used to measure the thermal conductance across the Ga^+-implanted region of the Si, the details and analyses for which are described in detail elsewhere.[45−47] In our specific experiments, the pump and probe $1/e^2$ radii are 29 and 7.5 μm, respectively, ensuring nearly one-dimensional heating during our TDTR measurements. To avoid any annealing of the samples, TDTR experiments were performed at ∼300 K with a maximum steady-state temperature rise of <1 K, as determined by solving the heat diffusion equation for the surface temperature of a multilayer sample. As the goal in this work is to resolve the changes in thermal conduction of the implanted region of the Si, and since this implanted region is restricted to $d \approx$ 10−75 nm beneath the Si surface (cf. TEM images—see Figure 1), we report all thermal conductances using a relatively high pump-modulation frequency for TDTR measurements (8.8 MHz) to ensure increased sensitivity to the thermal resistance near the silicon surface. We treat the entire Ga^+-implanted region as an interface in our thermal analysis, fitting for the effective thermal boundary conductance (TBC) across the Al/Si interface in our analysis using a two-layer model. The effective thermal conductivities derived from the measured TBC data are calculated by multiplying the measured conductances by the damaged depth obtained from TEM analyses. However, given the effective thermal conductivities reported are around ∼1 W/(m K), the thermal penetration depth into this layer would be $L_z \approx$ 150 nm. Thus, the ratio of thermal penetration depth is $L_z/d \approx$ 2−15, putting some samples in a regime where the treatment of the Ga^+-implanted region as an interface is ambiguous.[27] As such, for samples having $L_z/d >$ 4.24, we additionally analyze the TDTR data treating the Ga^+-implanted region as a thin film using a three-layer model and fitting for the thermal conductivity of the thin film directly. We find agreement between the two methods within 10% of the reported values, within experimental uncertainty. Additionally, all trends are preserved using this analysis. In both cases, due to the relatively small thickness of the Ga^+-implanted region, the intrinsic thermal conductivity of the implanted region cannot be explicitly measured separately from the Al/Ga^+-implanted region and Ga^+-implanted region/Si substrate interfaces. Thus, these interfacial thermal conductances are intrinsically included in the effective thermal conductivity reported. However, based on previous reported values for TBCs for Al/a-Si and a-Si/Si of similar film thicknesses,[32] (1) the thermal conductivity of the Ga^+-implanted region will dominate the overall conductance and (2) the Al/a-Si and a-Si/Si TBC will be relatively constant for varying thicknesses, so that any changes in effective thermal conductivities can be attributed to the Ga^+ region rather than the interfaces. However, based on previous reported values for TBCs for Al/a-Si and a-Si/Si of similar film thicknesses,[32] the combined total thermal boundary conductance from both interfaces is ∼100−200 MW/m^2/K. For doses >10^{14} Ga^+/cm^2, the measured conductance is an order of magnitude lower than this, meaning to total thermal resistance is dominated by the Ga^+-implanted region. Moreover, this previous study suggests that the combined thermal boundary resistance will be relatively constant for varying thicknesses, so that any changes in effective thermal conductivities can be attributed to the Ga^+ region rather than the interfaces. Thus, although the interfacial thermal resistance can be significant for doses <10^{14} Ga^+/cm^2, any differences in the measured conductance shown in Figure 1 are attributed to changes in thermal conductivity due to Ga^+ ion irradiation, and therefore capture the implications of Ga^+ irradiation on thermal conductivity of the irradiated region.

Results were not dependent on the Ga^+ current levels chosen for irradiation. The Ga^+ FIB instrument used in this work utilizes a single Ga^+ source operated with an extraction voltage of 30 kV, i.e., all ions impact the surface with a constant energy. Currents are varied by changing a physical aperture that is in-line with the source. Therefore, only the area, over which Ga^+ impact the surface, is modified when changing the instrument's current. To verify that no difference exists when changing currents, experiments were run at constant doses with varying currents. TBC values for all experiments were all within the error of commensurate measurements.

Carbonaceous layers can form in an SEM/FIB vacuum chamber due to the organic contamination.[48,49] To ensure a lack of a carbonaceous film in this work, a set of samples are treated with oxygen radicals and compared with other control samples. Five control samples are measured in this work. Three of these samples were treated with oxygen radicals and the other two were not. This process was performed in the same chamber used for doping samples. The samples are treated by O radicals for half an hour. The setting, according to the manufacturer, minimizes the effects of surface damage by O atoms and oxidization of Si, whereas O radicals chemically attack possible organic contaminants. These samples were characterized using TDTR, as described previously. The samples postprocessed by O radicals have a effective thermal conductivity that is 7% higher than those that were unprocessed. This 7% change could be associated to either a change in the chemistry of the surface or removing some impurities. However, this topic is beyond the scope of this work. Accordingly, any erroneous effects of possible residues, in the setup, aside the Ga doping are expected to be smaller than 7%, which is within the margin of error for this report.

Transmission Electron Microscope (TEM) Characterization. TEM cross-sections were created using the same Ga^+ FIB used to create the samples. Cross-sections were placed on a TEM grid and cleaned and imaged using a Titan 80-300 ST from Thermo-Fisher Scientific. An accelerating voltage of 300 keV was used, and images were collected using a model US1000 CCD Camera from Gatan, Inc.

AUTHOR INFORMATION

Corresponding Author

*E-mail: zleseman@ksu.edu.

ORCID

S. Rempe: 0000-0003-1623-2108
A. Giri: 0000-0002-8899-4964
C. J. Szwejkowski: 0000-0002-1354-4416
J. T. Gaskins: 0000-0001-8622-5902
Z. C. Leseman: 0000-0002-9846-7164

Author Contributions

S.A. designed the masks for processing, assisted in the photolithography processing, prepared the irradiated samples, and wrote the first draft of the manuscript. Y.-B.J., M.G.B., S.R., D.H.A., and S.A. prepared the TEM samples and performed the TEM analyses. B.F.D., A.G., C.J.S., J.T.G., and J.B. conducted the thermal measurements and analyses. M.M.M.E. performed the photolithography processing and the deposition of Al films. D.F.G. was involved with irradiation of the samples and initially designed the method of sample preparation. P.E.H. oversaw thermal characterization of samples and contributed to the discussion and interpretation of the results. Z.C.L. proposed the idea for the article, oversaw: preparation of samples, processing, microscopy, and interpretation of the results. All authors reviewed the manuscript. Z.C.L. was the final editor of the article.

Notes

The authors declare no competing financial interest.

ACKNOWLEDGMENTS

S.A., M.G.B., D.F.G., and Z.C.L. acknowledge support from the National Science Foundation Division of CMMI under Award 1056077. Materials supplied by P.E.H. et al. are based upon work partially supported by the Air Force Office of Scientific

DOI: 10.1021/acsami.8b11949
ACS Appl. Mater. Interfaces 2018, 10, 37679−37684

Research under award number FA9550-18-1-0352. P.E.H. is also appreciative for support from the National Science Foundation, Grant no. CBET-1706388.

REFERENCES

(1) Ju, Y. S.; Goodson, K. E. Phonon Scattering in Silicon Films with Thickness of Order 100 nm. *Appl. Phys. Lett.* **1999**, *74*, 3005−3007.
(2) Asheghi, M.; Touzelbaev, M. N.; Goodson, K. E.; Leung, Y. K.; Wang, S. S. Temperature-Dependent Thermal Conductivity of Single-Crystal Silicon Layers in SOI Substrates. *J. Heat Transfer* **1998**, *120*, 30−36.
(3) Ferrando-Villalba, P.; Lopeandia, A. F.; Abad, Ll; Llobet, J.; Molina-Ruiz, M.; Garcia, G.; Gerbolès, M.; Alvarez, F. X.; Goñi, A. R.; Munoz-Pascual, F. J.; et al. In-Plane Thermal Conductivity of Sub-20 nm Thick Suspended Mono-Crystalline Si Layers. *Nanotechnology* **2014**, *25*, No. 185402.
(4) Yu, J.-K.; Mitrovic, S.; Tham, D.; Varghese, J.; Heath, J. R. Reduction of Thermal Conductivity in Phononic Nanomesh Structures. *Nat. Nanotechnol.* **2010**, *5*, 718−721.
(5) Tang, J.; Wang, H.; Lee, D. H.; Fardy, M.; Huo, Z.; Russell, T. P.; Yang, P. Holey Silicon as an Efficient Thermoelectric Material. *Nano Lett.* **2010**, *10*, 4279−4283.
(6) Hochbaum, A. I.; Chen, R.; Delgado, R. D.; Liang, W.; Garnett, E. C.; Najarian, M.; et al. Enhanced Thermoelectric Performance of Rough Silicon Nanowires. *Nature* **2008**, *451*, 163−165.
(7) Loureiro, J.; Mateus, T.; Filonovich, S.; Ferreira, M.; Figueira, J.; Rodrigues, A.; Donovan, B. F.; Hopkins, P. E.; Ferreira, I. Hydrogenated Nanocrystalline Silicon Thin Films with Promising Thermoelectric Properties. *Appl. Phys. A: Mater. Sci. Process.* **2015**, *120*, 1497−1502.
(8) Kim, B.; Nguyen, J.; Reinke, C.; Shaner, E.; Harris, C. T.; El-Kady, I.; Iii, R. H. O. Thermal Conductivity Manipulation in Lithographically Patterned Single Crystal Silicon Phononic Crystal Structures. *IEEE Int. Ultrason. Symp. Proc.* **2011**, 1308−1311.
(9) Alaie, S.; Goettler, D. F.; Abbas, K.; Su, M. F.; Reinke, C. M.; El-Kady, I.; Leseman, Z. C. Microfabricated Suspended Island Platform for the Measurement of In-Plane Thermal Conductivity of Thin Films And Nanostructured Materials With Consideration of Contact Resistance. *Rev. Sci. Instrum.* **2013**, *84*, No. 105003.
(10) Alaie, S.; Goettler, D. F.; Su, M.; Leseman, Z. C.; Reinke, C. M.; El-Kady, I. Thermal Transport in Phononic Crystals and the Observation of Coherent Phonon Scattering at Room Temperature. *Nat. Commun.* **2015**, *6*, No. 7228.
(11) Alaie, S.; Goettler, D. F.; Jiang, Y.-B.; Abbas, K.; Baboly, M. G.; Anjum, D. H.; Chaieb, S.; Leseman, Z. C. Thermal Conductivity and Nanocrystalline Structure of Platinum Deposited by Focused Ion Beam. *Nanotechnology* **2015**, *26*, No. 085704.
(12) Hopkins, P. E.; Reinke, C. M.; Su, M. F.; Iii, R. H. O.; Shaner, E. A.; Leseman, Z. C.; Serrano, J. R.; Phinney, L. M.; El-Kady, I. Reduction in the Thermal Conductivity of Single Crystalline Silicon by Phononic Crystal Patterning. *Nano Lett.* **2011**, *11*, 107−112.
(13) Goettler, D. F.; Su, M. F.; Reinke, C. M.; Alaie, S.; Hopkins, P. E.; Olsson, R. H.; El-Kady, I.; Leseman, Z. C. Realization of a 33 GHz Phononic Crystal Fabricated in a Freestanding Membrane. *AIP Adv.* **2011**, *1*, No. 042001.
(14) Li, D.; Wu, Y.; Kim, P.; Shi, L.; Yang, P.; Majumdar, A. Thermal Conductivity of Individual Silicon Nanowires. *Appl. Phys. Lett.* **2003**, *83*, 2934−2936.
(15) Marconnet, A. M.; Kodama, T.; Asheghi, M.; Goodson, K. E. Phonon Conduction in Periodically Porous Silicon Nanobridges. *Nanoscale Microscale Thermophys. Eng.* **2012**, *16*, 199−219.
(16) Kivinen, P.; Savin, A.; Zgirski, M.; Törmä, P.; Pekola, J.; Prunnila, M.; Ahopelto, J. Electron − Phonon Heat Transport and Electronic Thermal Conductivity in Heavily Doped Silicon-On-Insulator Film. *J. Appl. Phys.* **2003**, *94*, 3201−3205.
(17) Sota, T.; Suzuki, K. Thermal Conductivity of Heavily Doped N-Type Si. *Phys. Status Solidi* **1991**, *163*, K5−K7.
(18) Cheaito, R.; Duda, J. C.; Beechem, T. E.; Hattar, K.; Ihlefeld, J. F.; Medlin, D. L.; Rodriguez, M. A.; Campion, M. J.; Piekos, E. S.; Hopkins, P. E. Experimental Investigation of Size Effects on the Thermal Conductivity of Silicon-Germanium Alloy Thin Films. *Phys. Rev. Lett.* **2012**, *109*, No. 195901.
(19) Chen, P.; Katcho, N. A.; Feser, J. P.; Li, W.; Glaser, M.; Schmidt, O. G.; Cahill, D. G.; Mingo, N.; Rastelli, A. Role of Surface-Segregation-Driven Intermixing on the Thermal Transport Through Planar Si/Ge Superlattices. *Phys. Rev. Lett.* **2013**, *111*, No. 115901.
(20) Cahill, D. G.; Watanabe, F. Thermal Conductivity of Isotopically Pure And Ge-Doped Si Epitaxial Layers From 300 To 550 K. *Phys. Rev. B* **2004**, *70*, No. 235322.
(21) Cahill, D. G.; Watanabe, F.; Rockett, A.; Vining, C. B. Thermal Conductivity of Epitaxial Layers of Dilute SiGe Alloys. *Phys. Rev. B - Condens. Matter Mater. Phys.* **2005**, *71*, No. 235202.
(22) Khizroev, S.; Litvinov, D. Focused-Ion-Beam-Based Rapid Prototyping of Nanoscale Magnetic Devices. *Nanotechnology* **2004**, *15*, R7−R15.
(23) Savenko, A.; Yildiz, I.; Petersen, D. H.; Bøggild, P.; Bartenwerfer, M.; Krohs, F.; Oliva, M.; Harzendorf, T. Ultra-High Aspect Ratio Replaceable AFM Tips Using Deformation-Suppressed Focused Ion Beam Milling. *Nanotechnology* **2013**, *24*, No. 465701.
(24) Mavrokefalos, A.; Nguyen, N. T.; Pettes, M. T.; Johnson, D. C.; Shi, L. In-Plane Thermal Conductivity of Disordered Layered WSe_2 and $(W)_X(WSe_2)_Y$ Superlattice Films. *Appl. Phys. Lett.* **2007**, *91*, No. 171912.
(25) Lee, S.-Y.; Kim, G.-S.; Lee, M.-R.; Lim, H.; Kim, W.-D.; Lee, S.-K. Thermal Conductivity Measurements of Single-Crystalline Bismuth Nanowires By the Four-Point-Probe 3-ω Technique at Low Temperatures. *Nanotechnology* **2013**, *24*, No. 185401.
(26) Fu, Y.; Bryan, N. K. A.; Shing, O. N. Characterization of Focused Ion Beam Induced Deposition Process And Parameters Calibration. *Sens. Actuators, A.* **2001**, *88*, 58−66.
(27) Liu, J.; Zhu, J.; Tian, M.; Gu, X.; Schmidt, A.; Yang, R. Simultaneous Measurement of Thermal Conductivity and Heat Capacity of Bulk And Thin Film Materials Using Frequency-Dependent Transient Thermoreflectance Method. *Rev. Sci. Instrum.* **2013**, *84*, No. 034902.
(28) Chen, G. *Nanoscale Energy Transport And Conversion*; Oxford University Press, 2005.
(29) Chernatynskiy, A.; Clarke, D.; Phillpot, S. Handbook of Nanoscience, Engineering, and Technology. In *Electrical Engineering Handbook*, 3rd ed.; CRC Press, 2012; pp 545−572.
(30) Cahill, D. G.; Braun, P. V.; Chen, G.; Clarke, D. R.; Fan, S.; Goodson, K. E.; Keblinski, P.; King, W. P.; Mahan, G. D.; Majumdar, A.; Maris, H. J.; Phillpot, S. R.; Pop, E.; Shi, L. Nanoscale Thermal Transport. II. 2003−2012. *Appl. Phys. Rev.* **2014**, *1*, No. 011305.
(31) Lehrer, C.; Frey, L.; Petersen, S.; Ryssel, H. Limitations of Focused Ion Beam Nanomachining. *J. Vac. Sci. Technol., B: Microelectron. Nanometer Struct.* **2001**, *19*, 2533.
(32) Braun, J. L.; Baker, C. H.; Giri, A.; Elahi, M.; Artyushkova, K.; Beechem, T. E.; Norris, P. M.; Leseman, Z. C.; Gaskins, J. T.; Hopkins, P. E. Size Effects on the Thermal Conductivity of Amorphous Silicon Thin Films. *Phys. Rev. B* **2016**, *93*, No. 140201.
(33) Wingert, M. C.; Zheng, J.; Kwon, S.; Chen, R. Thermal Transport in Amorphous Materials: A Review. *Semicond. Sci. Technol.* **2016**, *31*, No. 113003.
(34) Carslaw, H. S.; Jaeger, J. C. *Conduction of Heat in Solids*; Oxford University Press: Oxford, 1959.
(35) Lee, D. N.; Lee, S. B. Solid-Phase Crystallization of Amorphous Silicon Films. *Adv. Top. Cryst.* **2015**, 15−19.
(36) Nickel, N. *Laser Crystallization of Silicon - Fundamentals to Devices*; Academic Press, 2003.
(37) Braun, J. L.; Hopkins, P. E. Upper Limit to the Thermal Penetration Depth During Modulated Heating of Multilayer Thin Films with Pulsed and Continuous Wave Lasers: A Numerical Study. *J. Appl. Phys.* **2017**, *121*, No. 175107.
(38) Volkert, C. A.; Minor, A. M. Focused Ion Beam Micromachining. *MRS Bull.* **2007**, *32*, 389−399.

DOI: 10.1021/acsami.8b11949
ACS Appl. Mater. Interfaces 2018, 10, 37679−37684

(39) Wada, H.; Kamijoh, T. Thermal Conductivity of Amorphous Silicon. *Jpn. J. Appl. Phys.* **1996**, *35*, L648−L650.
(40) Mayer, J.; Giannuzzi, L. A.; Kamino, T.; Michael. TEM Sample Preparation and FIB-Induced Damage. *MRS Bull.* **2007**, *32*, 400−407.
(41) Michael, J. R. Understanding Microstructural Changes in Metal Induced by Gallium Ion Beam Irradiation. *Microsc. Microanal.* **2013**, *19*, 884−885.
(42) Spolenak, R.; Sauter, L.; Eberl, C. Reversible Orientation-Biased Grain Growth in Thin Metal Films Induced by a Focused Ion Beam. *Scr. Mater.* **2005**, *53*, 1291−1296.
(43) Olliges, S.; Gruber, P.; Bardill, A.; Ehrler, D.; Carstanjen, H. D.; Spolenak, R. Converting Polycrystals into Single Crystals - Selective Grain Growth by High-Energy Ion Bombardment. *Acta Mater.* **2006**, *54*, 5393−5399.
(44) Callister, W. D. *Materials Science and Engineering*; 3rd ed.; Wiley: New York, 1994.
(45) Cahill, D. G. Analysis of Heat Flow in Layered Structures for Time-Domain Thermoreflectance. *Rev. Sci. Instrum.* **2004**, *75*, No. 5119.
(46) Schmidt, A. J. Pump-Probe Thermoreflectance. *Annu. Rev. Heat Transfer* **2013**, *16*, 159−181.
(47) Hopkins, P. E.; Serrano, J. R.; Phinney, L. M.; Kearney, S. P.; Grasser, T. W.; Harris, C. T. Criteria for Cross-Plane Dominated Thermal Transport in Multilayer Thin Film Systems During Modulated Laser Heating. *J. Heat Transfer* **2010**, *132*, No. 081302.
(48) Hopkins, P. E.; Hattar, K.; Beechem, T.; Ihlefeld, J. F.; Medlin, D. L.; Piekos, E. S. Reduction in thermal boundary conductance due to proton implantation in silicon and sapphire. *Appl. Phys. Lett.* **2011**, *98*, 231901.
(49) Hopkins, P. E.; Hattar, K.; Beechem, T.; Ihlefeld, J. F.; Medlin, D. L.; Piekos, E. S. Addendum: "Reduction in thermal boundary conductance due to proton implantation in silicon and sapphire". *Appl. Phys. Lett.* **2011**, *98*, 231901.

DOI: 10.1021/acsami.8b11949
ACS Appl. Mater. Interfaces 2018, 10, 37679−37684